Published in final edited form as:
J Endocrinol. 2019 March 01; 240(3): 483–496. doi:10.1530/JOE-18-0623.

Vagal afferents contribute to sympathoexcitation–driven metabolic dysfunctions

L. Francisco Lorenzo–Martín[1,2,3], **Mauricio Menacho–Márquez**[1,2,3,§], **Salvatore Fabbiano**[1,2,§], **Omar Al–Massadi**[4,5,6], **Antonio Abad**[1,2,3], **Sonia Rodríguez–Fdez**[1,2], **María A. Sevilla**[1,2], **María J. Montero**[1,2], **Carlos Diéguez**[4,5,6], **Rubén Nogueiras**[4,5,6], and **Xosé R. Bustelo**[1,2,*]

[1]Centro de Investigación del Cáncer, CSIC–University of Salamanca, 37007 Salamanca, Spain

[2]Instituto de Biología Molecular y Celular del Cáncer, CSIC–University of Salamanca, 37007 Salamanca, Spain

[3]Centro de Investigación Biomédica en Red de Cáncer (CIBER*ONC*), CSIC–University of Salamanca, 37007 Salamanca, Spain

[4]Departamento de Fisioloxía, University of Santiago de Compostela, 15782 Santiago de Compostela, Spain

[5]Centro de Investigación en Medicina Molecular e Enfermidades Crónicas, University of Santiago de Compostela, 15782 Santiago de Compostela, Spain

[6]Centro de Investigación Biomédica en Red de Cáncer sobre la Fisiopatología de la Obesidad y Nutrición (CIBER*OBN*), University of Santiago de Compostela, 15782 Santiago de Compostela, Spain

Abstract

Multiple crosstalk between peripheral organs and the nervous system are required to maintain physiological and metabolic homeostasis. Using Vav3–deficient mice as a model for chronic sympathoexcitation–associated disorders, we report here that afferent fibers of the hepatic branch of the vagus nerve are needed for the development of the peripheral sympathoexcitation, tachycardia, tachypnea, insulin resistance, liver steatosis, and adipose tissue thermogenesis present in those mice. This neuronal pathway contributes to proper activity of the rostral ventrolateral medulla, a sympathoregulatory brainstem center hyperactive in *Vav3*$^{-/-}$ mice. Vagal afferent inputs are also required for the development of additional pathophysiological conditions associated with

*Corresponding author: XRB (xbustelo@usal.es).
§Present address: **MM–M:** Laboratorio Max Planck de Biología Estructural, Química y Biofísica Molecular, Rosario, Argentina; **SF:** Département Physiologie Cellulaire et Métabolisme, Université de Genève, 1205 Genève, Switzerland.

Conflicts of Interest
The authors report no conflict of interest associated with this work.

Author Contributions
LFL–M participated in all the experimental work, analyzed data, performed artwork design and contributed to the writing of the manuscript. MM–M and SF initiated the study, performed animal–based work, and analyzed data. OA–M performed hepatic vagotomies. SR–F and AA carried out animal–related procedures. MAS and MJM help in the cardiovascular determinations and analyzed data. CD and RN helped participated in surgical procedures and analyzed data. XRB conceived the work, wrote the manuscript, and carried out the final editing of the figures.

Europe PMC Funders Author Manuscripts

deregulated rostral ventrolateral medulla activity. By contrast, they are dispensable for other peripheral sympathoexcitation–associated disorders sparing metabolic alterations in liver.

Keywords

Sympathetic system; ventrolateral medulla; brainstem; GABAergic signals; hypertension; metabolic syndrome; diabetes; liver; adipose tissue; thermogenesis

Introduction

Physiological and metabolic balance in the organism requires extensive crosstalk between the central nervous system and peripheral organs. Efferent signals to the periphery are mediated by the sympathetic (SNS) and parasympathetic branches of the autonomic nervous system, both of which cooperate to fine tune energy consumption rates, mobilization of energy stores, glucose metabolism, insulin production, and the real–time functional adaptability of many tissues to feeding, environmental and behavioral–associated changes (Saper 2002). For example, the stimulation of the SNS leads to mobilization of glucose from internal stores and gluconeogenesis, inhibition of insulin release, increased energy expenditure, adipose tissue–associated thermogenesis as well as to transient increases in blood pressure, ventilation activity, and vasomotor tone (Guyenet 2006; Lambert, et al. 2010). One of the key brainstem centers controlling the sympathetic outflow is the rostral ventrolateral medulla (RVLM) (Grill and Hayes 2012; Guyenet 2006; Saper 2002). On the other hand, the brain gets inputs from peripheral organs to rapidly react to the physiological and metabolic imbalances of the organism (Saper 2002). In the case of metabolic changes, this information is conveyed to multiple central and brainstem areas by afferent neurons sprouting from peripheral organs and by the long–range action of hormones (Grill and Hayes 2012). The understanding of these crosstalk is critical, since their alteration can cause or cooperate with other genetic and life style factors in the development of epidemiologically relevant diseases such as type 2 diabetes, obesity, and hypertension. All those diseases can come together in the same pathophysiological pack, as is the case of borderline hypertension, neurogenic hypertension, and the metabolic syndrome (Lambert et al. 2010; Mancia, et al. 2007; Moller and Kaufman 2005). This latter multiorgan spanning disease, together with the high incidence of sympathomimetic toxidrome owing to the increasing use of both legal and illegal sympathomimetics, is one the most important challenges faced by our health systems both in terms of epidemiological incidence and treatment costs (Dixon 2010). Unfortunately, the afferent signals that convey the metabolic information back to the brain and how such data are integrated, processed, and finally articulated into defined peripheral responses remain poorly characterized as yet. Current evidence suggests that the vagus, the longest and most complex cranial nerve that innervates most internal organs (Saper 2002), is probably a key element of these crosstalk. Thus, it has been reported that changes in glucose, protein, and lipid content in the hepatic portal circulation lead to the stimulation of afferent fibers of the hepatic vagal branch (Benthem, et al. 2000; Grekin, et al. 1995; Grill and Hayes 2012; Yi, et al. 2010). The use of genetically manipulated mice has shown that vagal afferent signals are also important to sustain the long–term development of glucocorticoid– and high fat–diet induced cardiovascular and

Europe PMC Funders Author Manuscripts

Europe PMC Funders Author Manuscripts

metabolic dysfunctions (Bernal-Mizrachi, et al. 2003; Bernal-Mizrachi, et al. 2007; Uno, et al. 2006; Yi et al. 2010). The final brain regions and mechanisms that integrate and translate these afferent signals into defined sympathetic–mediated peripheral effects have not been identified as yet.

In this work, we decided to analyze the role of the vagus nerve in diseases derived from a chronic and systemic sympathoexcitation condition. To this end, we utilized as working model knockout mice lacking expression of the Rho GTPase activator Vav3 (Bustelo 2014). These animals show defects in the migration and guidance of the axons of the GABAergic neurons located in the caudal ventrolateral medulla (CVML), a problem that leads to the loss of the tonic inhibition of the RVLM by GABAergic axons from that brainstem region (Fig. 1A) (Sauzeau, et al. 2010a). This defect causes peripheral sympathoexcitation in those mice and the progressive development of SNS–associated dysfunctions such as hypertension, hypertension–associated morbidities (e.g., cardiovascular remodeling, kidney fibrosis), tachycardia, tachypnea, liver steatosis, insulin resistance, hyperlipidemia, and cold–independent thermogenesis both in the white (WAT) and brown (BAT) adipose tissue (Fig. 1A). Importantly, these dysfunctions take place in the absence of any pharmacological treatment, obesity, or high fat–diet conditions (Menacho-Marquez, et al. 2013; Sauzeau et al. 2010a; Sauzeau, et al. 2006). Thus, these animals represent an ideal model to assess the role of the hepatic vagus on the evolution of systemic metabolic diseases associated with borderline hypertension, postreceptor insulin resistance, and obesity–independent metabolic syndrome. Using this model, we report here that the hepatic afferent fibers of the vagus play critical roles in the etiology of the wide spectrum of disorders associated with neurogenic–driven metabolic syndrome.

Materials and Methods

Ethical approval

All animal experiments were done according to protocols approved by the Bioethics Committees of the Universities of Salamanca and Santiago de Compostela.

Animal studies

Male *Vav3*$^{-/-}$ and *Vav2*$^{-/-}$ C57BL/10 mice (Doody, et al. 2001; Sauzeau et al. 2006) were kept in ventilated rooms in pathogen–free facilities under controlled temperature (23ºC), humidity (50%), and illumination (12–hour–light/12–hour–dark cycle) conditions. After weaning, mice were fed a standard chow global diet #2918 (6.2% fat, 3.1 kcal/g; Harlan Laboratories).

Surgical subdiaphragmatic vagotomies

The surgical procedure was performed as previously described (Imbernon, et al. 2013; Imbernon, et al. 2016). Briefly, 2.5–month–old mice of the indicated genotypes under ketamine–xylazine anesthesia were placed on their backs and subjected to a midline abdominal incision. After carefully moving the liver to the right side of the animals, the dorsal and ventral branches of the vagus nerve were exposed, each branch ligated with surgical suture at two points as distally as possible to prevent bleeding, and then the area

between the two sutures was removed by cauterization. After this procedure, the liver was moved back to the normal anatomical position and both the abdominal muscles and the skin sutured. As control, we performed sham operations in which each trunk of the vagal nerve was exposed without ligation and cauterization. Physiological evaluations were conducted 21 days post–operative recovery. Animals were analyzed in vivo at the 30th and 45th day postsurgery and, eventually, euthanized when they were 4–month–old. Effectiveness of the vagotomy was assessed by post–mortem stomach observation of each experimental animals. Only mice showing an evident increase in stomach size after vagotomy (due to motoric dysfunction) were included in final analyses.

Blood pressure, heart rate, and breathing frequency determinations

These physiological parameters were determined as described elsewhere (Sauzeau et al., 2006; Sauzeau et al., 2010).

Glucose tolerance tests

These analyses were performed by injecting intraperitoneally D–glucose (2 g/kg body weight; Cat. number G6152, Sigma) in mice that had been previously fasted for 18 hours. Aliquots of the blood of the injected mice were then serially collected from tail bleeds every 30 min over a 3 hour–long period. Finally, the concentration of plasma glucose in those aliquots was determined using a glucometer (Accu–Check; Aviva, Roche). Areas under the curve values were determined as described (Menacho-Marquez et al. 2013).

Histological studies

Liver, BAT and white adipose tissue were extracted, fixed in 4% paraformaldehyde, included in paraffin, cut in 2–3 μm thick sections, and stained with hematoxylin/eosin. Images were captured using an BX51 microscope coupled to a DP70 digital camera (both from Olympus). Liver sections were blindly analyzed by an independent pathologist to classify them according to steatotic grade. Quantification of the number of brown adipocytes was done de visu by two individuals using unlabeled images from BAT histological sections.

Analysis of liver triglycerides

Total lipids were extracted for 4 hours using an 8:1 mixture of chloroform and methanol from liver samples (50 mg) from overnight fasted mice. The lipophilic fraction was obtained, mixed with 1 N H_2SO_4 (Sigma), centrifuged for 10 min, and the concentration of triglycerides present in the resulting supernatant determined enzymatically (Serum Triglyceride Determination Kit; Cat. numbers G7793, F6428 and T2449, Sigma).

mRNA abundance determinations

Total RNAs were extracted and quantitated as previously described by qRT–PCR (Citterio, et al. 2012). Primers used for this step included 5'–CGG TGT TGT GCG GTG TCT GTA GT–3' (forward for *Ppargc1a*), 5'–CGA TCA CCA TAT TCC AGG TCA AG–3' (reverse for *Ppargc1a*), 5'–TAG AGC ATA TCC CCC AGG TG–3' (forward for *Srbp1c*), 5'–GGT ACG GGC CAC AAG AAG TA–3' (reverse, *Srbp1c*), 5'–GAC CGT GGT GAT CCG CGG GG–3' (forward, *Insig2*), 5'–CTG AGG CTG TGC CGC AGC AT–3' (reverse, *Insig2*), 5'–

GGG CCC TTG TAA ACA ACA AA–3' (forward, *Ucp1*), 5'–GTC GGT CCT TCC TTG GTG TA–3' (reverse, *Ucp1*), 5'–TGC ACC ACC AAC TGC TTA GC–3' (forward, *Gapdh*), and 5'–TCT TCT GGG TGG CAG TGA TG–3' (reverse, *Gapdh*).

Brainstem immunohistochemistry

The brains were extracted, fixed in 4% paraformaldehyde, dissected at the brainstem level using a mouse brain slicer matrix (RBMA–200C, World Precision Instruments), paraffin embedded, cut in 2 μm thick sections, and scanned using an Olympus BX51 microscope coupled with a DotSlide system for the identification of RVLM. TH staining (dilution 1:50, Cat. Number 22941, ImmunoStar) was carried out using the Ventana Discovery system (Roche) and the following parameters: citrate buffer pH 6.0 for heat–induced antigen retrieval, 40 min incubations with primary and secondary (Cat. number ab133469, Abcam) antibodies, detection step with the ChromoMap DAB kit (Cat. number 760–159, Roche), and counterstaining with hematoxylin. The quantification of the number of RVLM TH^+ neurons was done using standard microscopy analyses.

Bicuculline treatments

Bicuculline (Cat. number: B9130, Sigma) was prepared in acid water and diluted (0.2 mg/ml) in sterile phosphate–buffered saline solution at the moment of the injection. 100 μl of that solution were injected intraperitoneally into mice 30 min before euthanasia (Menacho-Marquez et al. 2013).

Determination of plasma catecholamines

Mice were fasted overnight and euthanized the next morning. Upon euthanasia, blood samples were collected and the plasma concentration of noradrenaline (CatCombi ELISA, IBL) and adrenaline (CatCombi ELISA, IBL) determined using the indicated ELISA kits as previously described (Sauzeau et al. 2006).

Elimination of vagal afferents

We followed a previously described procedure to carry out these experiments (Bernal-Mizrachi et al. 2007). Hence, upon the surgical opening of the abdominal walls of ketamine–xylacine anesthetized mice of the indicated genotypes, the anterior ligament and the membranous connection of the left lobe of the liver to the diaphragm were cut to give better visibility of the esophageal–hepatic attachments. This region contains a neurovascular bundle including the hepatic branch of the vagus nerve. This branch was selectively exposed and, with the help of a gauze, soaked in capsaicin (Cat. number M2028, Sigma). To this end, a stock solution was first prepared by sonicating 10 mg of the toxin in 0.1 ml Tween 80 (Cat. number P4780, Sigma). Subsequently, the sonicated preparation was diluted in 0.9 ml of olive oil (Cat. number O1514, Sigma). To ensure the local action of the toxin, the capsaicin–treated bundles were wrapped up in Paraffin paper (Cat. number 80–6135–67, GE Healthcare) for 30 min. The application was repeated twice so that a total dose of 0.5 mg of capsaicin was applied to each experimental mouse. In the case of the sham–operated controls, the above procedure was performed using the carrier solution (Tween 80 in olive

oil, 1:10 dilution). Physiological evaluations were conducted 21 days post–operative recovery.

Determination of plasma glucocorticoids

Blood samples were collected as indicated for the determination of catecholamines. The concentration of cortisol and corticosterone in plasma was then determined using the appropriate Enzyme Immunoassay Kit (Cat. numbers K003–H1 and K014–H1, respectively; Arbor) as indicated by the manufacturer.

Statistics

Data normality and equality of variances were analyzed with Shapiro–Wilk and Bartlett's tests, respectively. Parametric distributions were analyzed using either one–way ANOVA or Student's *t* tests for comparison between two unpaired groups. Non–parametric distributions were analyzed using either Kruskal–Wallis or Mann–Whitney tests. Values were considered significant when $P \leq 0.05$.

Results

Complete vagotomy blocks sympathoexcitation–driven dysfunctions in mice

We performed both sham operations and complete subdiaphragmatic vagotomies on *Vav3*$^{-/-}$ mice to assess the contribution of the vagus nerve to the SNS–dependent disorders exhibited by those mice. The comprehensive characterization of the metabolic parameters of these mice has been reported before (Menacho-Marquez et al. 2013). As controls, we used wild–type (WT) and *Vav2*$^{-/-}$ mice subjected to the same surgical procedure. The inclusion of *Vav2*$^{-/-}$ mice, which lack a related Rho GTPase activator of the Vav family (Bustelo 2014), was of special interest because they show levels of catecholamines in the plasma comparable to those found in *Vav3*$^{-/-}$ mice. However, the sympathoexcitation of *Vav2*$^{-/-}$ mice is an indirect downstream consequence of their hypertensive state rather than being directly caused by deregulated RVLM activity (Sauzeau, et al. 2010b). As a consequence, and unlike the case of *Vav3*$^{-/-}$ mice, the sympathoexcitation of the Vav2–deficient animals can be eliminated by standard anti–hypertensive drugs (Sauzeau et al. 2010b). The use of these mice is also of interest because they develop tachycardia, systemic hypertension and associated comorbidities very similar to those found in *Vav3*$^{-/-}$ but, instead, do not exhibit tachypnea, fatty liver disease, insulin resistance or adipose tissue thermogenesis (Menacho-Marquez et al. 2013; Sauzeau, et al. 2007). Hence, the combined used of these two Vav family knockout mouse models allowed us to distinguish the effects of the complete liver vagotomy under different conditions of peripheral sympathoexcitation. We found that the resection of the vagus nerve in WT mice does not trigger any significant alteration in blood pressure (Fig. 1B), heart beat frequency (Fig. 1C), breathing activity (Fig. 1D), plasma glucose clearance (Fig. 1E,F), liver histology (Fig. 1G), and liver triglyceride content (Fig. 1H). This procedure does not promote either the thermogenic activity in the adipose tissue of WT mice, as exemplified by the lack of changes in brown adipose tissue (BAT) histology (Fig. 1I,J), the absence of elevated levels of both *Ppargc1a* and *Ucp1* mRNA levels in the BAT (data not shown, but see below Fig. 2F), and the low levels of the *Ucp1* transcript present in the white adipose tissue (WAT) when compared to sham operated controls (Fig.

1K). *Ppargc1* encodes Pgc1α (peroxisome proliferator–activated receptor γ coactivator 1 α), a transcriptional factor required for *Ucp1* expression in adipose tissues. *Ucp1* encodes a protein involved in the uncoupling of the oxidative phosphorylation from the respiratory chain, a process that allows the dissipation of energy as heat (Cannon and Nedergaard 2004). By contrast, we observed that the complete subdiaphragmatic vagotomy eliminates the hypertension (Fig. 1B), the tachycardia (Fig. 1C), the tachypnea (Fig. 1D), the increased glucose intolerance (Fig. 1E,F), the liver steatosis (Fig. 1G,H) as well as the histological (Fig. 1I,J) and functional (Fig. 1K) features associated with increased adipose tissue heat dissipation typically observed in *Vav3*$^{-/-}$ mice (Menacho-Marquez et al. 2013; Sauzeau et al. 2010a; Sauzeau et al. 2006). These effects are specifically linked to the phenotype of *Vav3*$^{-/-}$ mice, because the resection of the subdiaphragmatic vagus nerve does not abolish the high blood pressure (Fig. 1B) and increased heart beat activity (Fig. 1C) exhibited by *Vav2*$^{-/-}$ mice. As in the case of WT animals, the rest of parameters tested in this study that were within normal physiological ranges in Vav2–deficient mice do not change upon the removal of the hepatic vagal branch (Fig. 1D–K).

Vav3 deficiency–triggered RVLM hyperactivation requires vagal nerve function

Given the connection of the pathophysiology of *Vav3*$^{-/-}$ mice with the hyperactivation of the RVLM, we next evaluated the effect of the complete subdiaphragmatic vagotomy on the RVLM–dependent sympathoexcitation present in these mice. To this end, we first quantified the number of neurons in the RVLM that were positive for tyrosine hydroxylase (TH), the limiting enzyme in the catecholamine biosynthetic route that is conventionally used as a marker for increased activity in catecholaminergic neurons (Molinoff and Axelrod 1971). As expected from the results obtained with nonmanipulated *Vav3*$^{-/-}$ mice (Sauzeau et al. 2010a), we found that the sham–operated *Vav3*$^{-/-}$ animals exhibit increased TH reactivity in RVLM cells when compared to WT controls (Fig. 2A–C). This indicates that the catecholaminergic cells in this area become activated under these conditions. However, such a reactivity drops down to WT–like levels in the case of vagotomized *Vav3*$^{-/-}$ animals (Fig. 2B,C). Concurring with this observation, the plasma levels of catecholamines become reduced in the latter animals to concentrations similar to those found in sham operated control mice (Fig. 2D). The complete vagotomy also eliminated the basal upregulation of SNS–regulated mRNA transcripts connected to the development of a metabolic syndrome conditions in the liver (Fig. 2E, compare light and dark red bars) (Menacho-Marquez et al. 2013). Those include, for example, the transcripts encoding Pgc1α, a transcriptional factor that favors insulin resistance through the TRB3–dependent inhibition of the phosphatidylinositol 3 kinase α (PI3Kα)–Akt pathway; Srebp1 (sterol regulatory element–binding protein 1), a transcriptional factor involved in the induction of de novo lipogenesis and steatosis programs in the liver; and Insig2 (insulin–induced gene 2), a negative regulator of Srebp1 that can be positively and negatively regulated by peroxisome proliferator–activated receptor α (Pparα) and the PI3Kα–Akt route, respectively (Dong and Tang 2010; Fernandez-Marcos and Auwerx 2011; Shao and Espenshade 2012). The complete subdiaphragmatic vagotomy also eliminates the high levels of the *Ppargc1a* and *Ucp1* transcripts typically observed in the BAT of *Vav3*$^{-/-}$ mice (Fig. 3F, compare light and dark red bars). By contrast, in agreement with the results shown in Figure 1, the vagotomy does not alter the low numbers of RVLM TH^{+} cells (Fig. 2B,C), the physiological plasma

concentrations of catecholamines (Fig. 2D) or the abundance of the interrogated liver (Fig. 2E) and BAT (Fig. 2F) transcripts in the case of WT mice. It also spares the high concentrations of plasma catecholamines that are normally displayed by *Vav2*$^{-/-}$ mice (Fig. 2D).

We have previously shown that the stereotaxic administration of the GABAergic antagonist bicuculline into the RVLM of WT mice phenocopies the *Vav3* gene deficiency in terms of sympathoexcitation and the ensuing elevation of blood pressure, heart, and respiratory rates (Sauzeau et al. 2010a). The same effects are found when low doses of bicuculline are intraperitoneally administered to mice. Such treatments also result in the induction of *Vav3*$^{-/-}$ mice–like histological and molecular changes in both the liver and BAT of the WT mice (Menacho-Marquez et al. 2013). By contrast, the stereotaxic or the intraperitoneal administration of bicuculline does not alter any of the SNS–associated pathophysiological alteration present in *Vav3*$^{-/-}$ mice given that these animals have already lost most of the inhibitory GABAergic wiring from the CVML to the RVLM (Menacho-Marquez et al. 2013; Sauzeau et al. 2010a). These observations led us to test the effects of the complete subdiaphragmatic vagotomy on the sympathoexcitation triggered by this $GABA_A$ receptor antagonist. Consistent with our previous results (Menacho-Marquez et al. 2013), we found that bicuculline prompts a rapid increase in RVLM TH^+ cells (Fig. 2B,C), plasma catecholamine levels (Fig. 2D) as well as the abundance of the liver (Fig. 2E) and BAT (Fig. 2F) transcripts in WT mice. Interestingly, all those bicuculine–mediated effects are abrogated in the case of the vagotomized counterparts (Fig. 1B–F). As expected, the administration of bicuculline does not have any effect on the already high levels of those physiological and molecular parameters present in *Vav3*$^{-/-}$ mice (Fig. 2B–F). It does not eliminate the effects of the vagotomy on the physiology of *Vav3*$^{-/-}$ mice (Fig. 2B–F). Collectively, these results indicate that the vagus is required for the sympathoexcitation–associated disorders chronically and acutely induced by the Vav3 deficiency and the bicuculline treatments, respectively.

Afferent vagal fibers maintain RVLM–driven sympathoexcitation in *Vav3*$^{-/-}$ mice

The foregoing data suggested that the effect of the vagotomy had to be related to the elimination of afferent vagal inputs that deliver metabolic information from peripheral tissues to the brainstem. To address this possibility, we next eliminated the unmyelinated afferent fibers of the vagus in *Vav3*$^{-/-}$ and control mice using topical applications of the neurotoxin capsaicin. It has been shown before that this procedure ensures the preservation of the efferent vagal fibers as well as the afferent fibers that travel through the posterior vagal trunk (Bernal-Mizrachi et al. 2007). As in the case of the surgical resection of the subdiaphragmatic vagus nerve (Fig. 2), we observed that the chemical ablation of these fibers results in a marked reduction in the usually high numbers of RVLM TH^+ cell (Fig. 3A,B) and plasma catecholamine levels (Fig. 3C,D) that are detected in *Vav3*$^{-/-}$ mice (Fig. 3A,B). In tone with the data obtained with complete subdiaphragmatic vagotomies (Fig. 2), we also found that the effects induced by capsaicin in *Vav3*$^{-/-}$ mice cannot be rescued by the subsequent administration of bicuculline (Fig. 3A–D). The administration of the neurotoxin does not have any effect on the low basal levels of RVLM TH^+ cells (Fig. 3A,B) and plasma catecholamines (Fig. 3C,D) present in WT mice. However, it does abrogate the stimulation

of RVLM TH^+ neurons (Fig. 3A,B) and the ensuing upregulation of plasma catecholamines (Fig. 3C,D) triggered by bicuculline in those animals. These results recapitulate again the data obtained using vagotomized WT animals (Fig. 2). Likewise, we observed that the chemical ablation of the vagal afferent fibers does not elicit any effect on the plasma catecholamine levels present in *Vav2*$^{-/-}$ mice (Fig. 3C,D).

Given that the elimination of the afferent fibers of the vagus hepatic branch blocks the hypertension and insulin resistance triggered by the administration of dexamethasone (Bernal-Mizrachi et al. 2007), we next investigated whether the foregoing results could be explained by a glucocorticoid–dependent phenotype of Vav3–deficient animals. Potentially in agreement with that possibility, we observed that the sham–operated *Vav3*$^{-/-}$ mice exhibit higher plasma levels of both cortisol (Fig. 3E) and corticosterone (Fig. 3F) when compared to mock operated WT controls. However, we observed that *Vav2*$^{-/-}$ mice, whose phenotype is not rescued by the removal of the hepatic branch of the vagus or its afferent fibers (Figs. 1 and 2), also display plasma concentrations of those two glucocorticoids quite similar to those observed in Vav3–deficient mice (Fig. 3E,F). The levels of corticoids in those two mouse strains do not change upon the removal of the afferent vagal fibers by capsaicin (Fig. 3E,F) or upon the resection of the entire subdiaphragmatic vagus nerve branch (Fig. 3G,H). Further arguing against a glucocorticoid–related cause, we observed that the elimination of either the afferent fibers (Fig. 3E,F) or the entire subdiaphragmatic (Fig. 3G,H) of the vagus nerve in WT mice cause in fact elevations in the plasma concentration of glucocorticoids comparable to those found in both sham– and vagotomized Vav family knockout mice. Yet, the WT animals do not develop a *Vav3*$^{-/-}$ mouse–like phenotype (Figs. 1–3). Collectively, these results rule out the possibility that the afferent pathway triggered by the Vav3–deficiency is owing to direct glucocorticoid–mediated effects in the liver. They also show that the chronic elevation of glucocorticoids within physiological ranges is not enough to trigger the previously described liver–specific and systemics effects of the dexamethasone treatments (Arner, et al. 1983; Bernal-Mizrachi et al. 2003).

Afferent vagal fibers contribute to SNS–driven dysfunctions in *Vav3*$^{-/-}$ mice

Consistent with the results from the previous section, we found that the elimination of the afferent fibers of the vagus hepatic branch restores the physiological levels of blood pressure (Fig. 4A), heart rates (Fig. 4B), and breathing activity (Fig. 4C) in Vav3–deficient animals. It also eliminates their metabolic syndrome condition, as demonstrated by their fully physiological responses to glucose infusion (Fig. 4D,E) as well as by the WT–like levels of both triglycerides (Fig. 4F) and metabolic syndrome–associated transcripts (*Ppragc1a*, *Srbep1c* and *Insig2*) (Fig. 4G) in the liver of those animals. In line with the results found in both Figures 2 and 3, the normal abundance of these transcripts in afferent fiber–depleted *Vav3*$^{-/-}$ mice is maintained even upon the administration of bicuculline (Fig. 4G). The ablation of the vagal afferents also abates the bicuculline–mediated induction of those three transcripts in the liver of WT mice (Fig. 4G). Further analyses revealed that the capsaicin treatment also blocks the expression of the *Ucp1* mRNA in the WAT of *Vav3*$^{-/-}$ mice (Fig. 4H), indicating that the SNS–driven browning typically observed in these mice also requires cooperation from vagal afferent fibers from the liver. As control, we did not find any statistically significant effect of capsaicin on the hypertensive (Fig. 4A) and tachycardic

(Fig. 4B) condition present in *Vav2*$^{-/-}$ mice (Sauzeau et al. 2007; Sauzeau et al. 2010b). Unlike the foregoing cases, we found that the elimination of the afferent fibers of the vagus does not eliminate the thermogenic–associated features of the BAT of *Vav3*$^{-/-}$ mice (Fig. 4I–K). This response is however blocked in animals in which the vagus was cauterized (Fig. 1I–K), suggesting that the foregoing remaining activity could be due to myelinated afferent fibers that survived the capsaicin treatment. In line with this, we have observed that capsaicin–treated *Vav3*$^{-/-}$ still display slightly elevated levels of plasma catecholamines when compared to WT mice and fully vagotomized *Vav3*$^{-/-}$ animals (compare Figs. 2D and 3C,D). Taken together, these results indicate that vagal afferent signals are needed for the development of the RVLM– and SNS–driven dysfunctions present in *Vav3*$^{-/-}$ mice (Fig. 4L). This requirement is independent of previously described vagal afferent fiber–dependent dysfunctions, such as the spurious activation of glucocorticoid pathways or high fat diet–induced obesity (Bernal-Mizrachi et al. 2003; Bernal-Mizrachi et al. 2007; Uno et al. 2006). Our results also indicate that this afferent input is dispensable for sustaining the tachycardia, hypertension and peripheral sympathoexcitation of *Vav2*$^{-/-}$ mice as well as the long–term metabolic homeostasis of WT animals.

Discussion

We have demonstrated here that signals conveyed by the afferent vagal fibers of the liver to the RVLM contribute to the development of a wide spectrum of pathophysiological disorders commonly associated with chronic sympathoexcitation. Importantly, our experiments indicate that the requirement of this afferent wiring applies to neurogenic–based but not to peripheral sympathoexcitation–associated disorders such as those present in *Vav2*$^{-/-}$ mice. Consistent with this, we have found that this vagal afferent connection is engaged during physiological (loss of GABAergic inhibitory wiring in Vav3–deficient mice) and pharmacological (e.g., bicuculline treatments in WT mice) conditions connected to unregulated RVLM activity. Importantly, our results also dissociate the contribution of this neuronal liver–RVLM axis from metabolic dysfunctions that could interfere with the interpretation of the mechanism involved such as obesity or abnormal levels of adrenal cortex activity. We have also observed that the overall vagus is not required for maintaining metabolic homeostasis in WT mice, a result that concurs with previous data from both experimental animals and liver transplanted patients in which the vagus is lost during surgery (Bernal-Mizrachi et al. 2007; Yi et al. 2010). This is probably due to the existence of mechanisms that compensate the loss of this afferent neuronal axis under normal physiological conditions. It remains to be determined whether such compensations still apply upon subjecting the mice to physiological challenges such as, for example, hypoglucemic conditions.

Although the contribution of the afferent vagal fibers to the phenotype of *Vav3*$^{-/-}$ mice does not rely on abnormal glucocorticoid function, our results indicate that the sympathoexcitation and dexamethasone signals processed through the hepatic afferent fibers share molecular and physiological features. Thus, *Vav3*$^{-/-}$ mice contain in their steatotic livers high levels of Pparα (Menacho-Marquez et al. 2013), one of the key executors of the metabolic program activated by glucocorticoids in the liver (Bernal-Mizrachi et al. 2003). Conversely, the ectopic expression of the glucocorticoid–connected Pparα and Pparγ2

proteins in the liver of mice promotes sympathoexcitation, hypertension, and adipocyte thermogenesis similar to those found in *Vav3*$^{-/-}$ mice (Bernal-Mizrachi et al. 2003; Uno et al. 2006). Given our current data, we hypothesize that the glucocorticoid–dependent vagal afferent pathway eventually impacts on RVLM sympathoregulatory activity. The shared features of *Vav3*$^{-/-}$, dexamethasone–treated, and Ppar family–expressing mice are also probably the consequence of the downstream activation of common fatty acid oxidation and gluconeogenic programs in the liver (Bernal-Mizrachi et al. 2003; Menacho-Marquez et al. 2013; Uno et al. 2006). Given the absence of vagal fibers in the liver parenchyma in rodents (Berthoud and Neuhuber 2000), it is likely that these metabolic changes generate metabolites that will stimulate the afferent vagal fibers located in the porta triads. This is consistent with previous reports indicating that the portal infusion of the long–chain fatty acid oleate triggers sympathetic activation, high blood pressure, tachycardia, and insulin resistance in rats (Benthem et al. 2000; Grekin, et al. 1997; Grekin et al. 1995). However, we cannot rule out at this point the contribution of other subdiagraphamatic tissues such as, for example, the intestine (see below).

The transmission to, and subsequent integration of these signals in the RVLM remains to be determined. The main point of innervation of the vagus nerve is the nucleus of the solitary tract (NTS) (Grill and Hayes 2012; Saper 2002), the region directly involved in the stimulation of the RVLM (Grill and Hayes 2012; Guyenet 2006; Saper 2002). The most usual mechanism to achieve this effect is the NTS–mediated elimination of the tonic GABAergic signals emitted by the CVLM (Grill and Hayes 2012; Guyenet 2006). It is possible, however, that the afferent signals transmitted by the vagus could be directly conveyed to the RVLM through other NTS neuronal subsets or indirectly via other brain areas such as the parvocellular autonomic neurons or the raphe pallidus (Guyenet 2006).

Most peripheral signals received by the RVLM result in sympathoinhibition (Guyenet 2006; Heesch 1999). However, it is worth noting that old reports have noticed that the stimulation of the afferent abdominal vagus, a branch that eventually converges with the hepatic vagus trunk, leads to the stimulation of the RVLM in conscious rabbits (Gieroba and Blessing 1994). Esophageal distension signals also stimulate afferent vagal fibers to elevate blood pressure in a RVLM–dependent manner in rabbits and cats. This response is inhibited by the electric stimulation of the aortic depressor nerve, suggesting that they converge at the NTS (Gieroba, et al. 1995). Emesis, which is initiated by activation of upper gastrointestinal vagal afferents that signal into the NTS, also increases blood pressure in both cancer patients subjected to chemotherapy and experimentally manipulated animal models (Carpenter 1990). It is feasible therefore that many afferent vagal fibers from the abdominal area, including the liver itself, could cooperatively intersect at the RVLM. This must be tissue– and stimulus–specific in any case, since some gastrointestinal hormones elicit RVLM sympathoinhibition using the same afferent bundles (Sartor and Verberne 2002). Given the involvement of the RVLM in the “sensing” of local variations of glucose (Grill and Hayes 2012; Verberne, et al. 2014), the present results further underscore the role of this brainstem sympathoregulatory center in metabolic control. They also suggest that the pharmacological targeting of this liver–RVLM neuronal axis might represent a potential avenue to treat patients with metabolic syndrome associated with either primary or secondary RVLM hyperactivity. Drugs targeting this axis, like optimized derivatives of the currently available

sympathodepressor imidazoline receptor agonists (Edwards, et al. 2012), could be adequate tools to achieve that aim.

Acknowledgements

We thank C. García–Macías for expert histological analyses and M. Blázquez, T. Teixeira, and S. Fraile for technical assistance. XRB is supported by grants from the Castilla–León Government (CSI252P18, CLC–2017–01), the Spanish Ministry of Science, Innovation and Universities (MSIU) (SAF2015–64556–R), Worldwide Cancer Research (14–1248), the Ramón Areces Foundation, and the Spanish Association against Cancer (GC16173472GARC). XRB's institution is supported by the Programa de Apoyo a Planes Estratégicos de Investigación de Estructuras de Investigación de Excelencia of the Ministry of Education of the Castilla–León Government (CLC–2017–01). SR–F and LFL–M contracts have been supported by funding from the MISIU (BES–2013–063573) and the Spanish Ministry of Education, Culture and Sports (LFL–M, FPU13/02923), respectively. Both Spanish and Castilla–León government–associated funding is partially supported by the European Regional Development Fund.

References

Arner P, Gunnarsson R, Blomdahl S, Groth CG. Some characteristics of steroid diabetes: a study in renal-transplant recipients receiving high-dose corticosteroid therapy. Diabetes Care. 1983; 6:23–25.

Benthem L, Keizer K, Wiegman CH, de Boer SF, Strubbe JH, Steffens AB, Kuipers F, Scheurink AJ. Excess portal venous long-chain fatty acids induce syndrome X via HPA axis and sympathetic activation. Am J Physiol Endocrinol Metab. 2000; 279:E1286–1293. [PubMed: 11093916]

Bernal-Mizrachi C, Weng S, Feng C, Finck BN, Knutsen RH, Leone TC, Coleman T, Mecham RP, Kelly DP, Semenkovich CF. Dexamethasone induction of hypertension and diabetes is PPAR-alpha dependent in LDL receptor-null mice. Nat Med. 2003; 9:1069–1075. [PubMed: 12847522]

Bernal-Mizrachi C, Xiaozhong L, Yin L, Knutsen RH, Howard MJ, Arends JJ, Desantis P, Coleman T, Semenkovich CF. An afferent vagal nerve pathway links hepatic PPARalpha activation to glucocorticoid-induced insulin resistance and hypertension. Cell Metab. 2007; 5:91–102. [PubMed: 17276352]

Berthoud HR, Neuhuber WL. Functional and chemical anatomy of the afferent vagal system. Auton Neurosci. 2000; 85:1–17. [PubMed: 11189015]

Bustelo XR. Vav family exchange factors: an integrated regulatory and functional view. Small GTPases. 2014; 5:9. [PubMed: 25483299]

Cannon B, Nedergaard J. Brown adipose tissue: function and physiological significance. Physiol Rev. 2004; 84:277–359. [PubMed: 14715917]

Carpenter DO. Neural mechanisms of emesis. Can J Physiol Pharmacol. 1990; 68:230–236. [PubMed: 2178747]

Citterio C, Menacho-Marquez M, Garcia-Escudero R, Larive RM, Barreiro O, Sanchez-Madrid F, Paramio JM, Bustelo XR. The rho exchange factors vav2 and vav3 control a lung metastasis-specific transcriptional program in breast cancer cells. Sci Signal. 2012; 5:ra71. [PubMed: 23033540]

Dixon JB. The effect of obesity on health outcomes. Mol Cell Endocrinol. 2010; 316:104–108. [PubMed: 19628019]

Dong XY, Tang SQ. Insulin-induced gene: a new regulator in lipid metabolism. Peptides. 2010; 31:2145–2150. [PubMed: 20817058]

Doody GM, Bell SE, Vigorito E, Clayton E, McAdam S, Tooze R, Fernandez C, Lee IJ, Turner M. Signal transduction through Vav-2 participates in humoral immune responses and B cell maturation. Nat Immunol. 2001; 2:542–547. [PubMed: 11376342]

Edwards LP, Brown-Bryan TA, McLean L, Ernsberger P. Pharmacological properties of the central antihypertensive agent, moxonidine. Cardiovasc Ther. 2012; 30:199–208. [PubMed: 21884003]

Fernandez-Marcos PJ, Auwerx J. Regulation of PGC-1alpha, a nodal regulator of mitochondrial biogenesis. Am J Clin Nutr. 2011; 93:884S–890. [PubMed: 21289221]

Gieroba ZJ, Blessing WW. Fos-containing neurons in medulla and pons after unilateral stimulation of the afferent abdominal vagus in conscious rabbits. Neurosci. 1994; 59:851–858.

Europe PMC Funders Author Manuscripts

Gieroba ZJ, Messenger JP, Blessing WW. Abdominal vagal stimulation excites bulbospinal barosensitive neurons in the rostral ventrolateral medulla. Neurosci. 1995; 65:355–364.

Grekin RJ, Dumont CJ, Vollmer AP, Watts SW, Webb RC. Mechanisms in the pressor effects of hepatic portal venous fatty acid infusion. Am J Physiol. 1997; 273:R324–330. [PubMed: 9249567]

Grekin RJ, Vollmer AP, Sider RS. Pressor effects of portal venous oleate infusion. A proposed mechanism for obesity hypertension. Hypertension. 1995; 26:193–198. [PubMed: 7607723]

Grill HJ, Hayes MR. Hindbrain neurons as an essential hub in the neuroanatomically distributed control of energy balance. Cell Metab. 2012; 16:296–309. [PubMed: 22902836]

Guyenet PG. The sympathetic control of blood pressure. Nat Rev Neurosci. 2006; 7:335–346. [PubMed: 16760914]

Heesch CM. Reflexes that control cardiovascular function. Am J Physiol. 1999; 277:S234–243. [PubMed: 10644250]

Imbernon M, Beiroa D, Vazquez MJ, Morgan DA, Veyrat-Durebex C, Porteiro B, Diaz-Arteaga A, Senra A, Busquets S, Velasquez DA, et al. Central melanin-concentrating hormone influences liver and adipose metabolism via specific hypothalamic nuclei and efferent autonomic/JNK1 pathways. Gastroenterol. 2013; 144:636–649 e636.

Imbernon M, Sanchez-Rebordelo E, Romero-Pico A, Kallo I, Chee MJ, Porteiro B, Al-Massadi O, Contreras C, Ferno J, Senra A, et al. Hypothalamic kappa opioid receptor mediates both diet-induced and melanin concentrating hormone-induced liver damage through inflammation and endoplasmic reticulum stress. Hepatol. 2016; 64:1086–1104.

Lambert GW, Straznicky NE, Lambert EA, Dixon JB, Schlaich MP. Sympathetic nervous activation in obesity and the metabolic syndrome--causes, consequences and therapeutic implications. Pharmacol Ther. 2010; 126:159–172. [PubMed: 20171982]

Mancia G, Bousquet P, Elghozi JL, Esler M, Grassi G, Julius S, Reid J, Van Zwieten PA. The sympathetic nervous system and the metabolic syndrome. J Hypertens. 2007; 25:909–920. [PubMed: 17414649]

Menacho-Marquez M, Nogueiras R, Fabbiano S, Sauzeau V, Al-Massadi O, Dieguez C, Bustelo XR. Chronic sympathoexcitation through loss of Vav3, a Rac1 activator, results in divergent effects on metabolic syndrome and obesity depending on diet. Cell Metab. 2013; 18:199–211. [PubMed: 23931752]

Molinoff PB, Axelrod J. Biochemistry of catecholamines. Annu Rev Biochem. 1971; 40:465–500. [PubMed: 4399447]

Moller DE, Kaufman KD. Metabolic syndrome: a clinical and molecular perspective. Annu Rev Med. 2005; 56:45–62. [PubMed: 15660501]

Saper CB. The central autonomic nervous system: conscious visceral perception and autonomic pattern generation. Annu Rev Neurosci. 2002; 25:433–469. [PubMed: 12052916]

Sartor DM, Verberne AJ. Cholecystokinin selectively affects presympathetic vasomotor neurons and sympathetic vasomotor outflow. Am J Physiol Regul Integr Comp Physiol. 2002; 282:R1174–1184. [PubMed: 11893623]

Sauzeau V, Horta-Junior JA, Riolobos AS, Fernandez G, Sevilla MA, Lopez DE, Montero MJ, Rico B, Bustelo XR. Vav3 is involved in GABAergic axon guidance events important for the proper function of brainstem neurons controlling cardiovascular, respiratory, and renal parameters. Mol Biol Cell. 2010a; 21:4251–4263. [PubMed: 20926682]

Sauzeau V, Jerkic M, Lopez-Novoa JM, Bustelo XR. Loss of Vav2 proto-oncogene causes tachycardia and cardiovascular disease in mice. Mol Biol Cell. 2007; 18:943–952. [PubMed: 17202406]

Sauzeau V, Sevilla MA, Montero MJ, Bustelo XR. The Rho/Rac exchange factor Vav2 controls nitric oxide-dependent responses in mouse vascular smooth muscle cells. J Clin Invest. 2010b; 120:315–330. [PubMed: 20038798]

Sauzeau V, Sevilla MA, Rivas-Elena JV, de Alava E, Montero MJ, Lopez-Novoa JM, Bustelo XR. Vav3 proto-oncogene deficiency leads to sympathetic hyperactivity and cardiovascular dysfunction. Nat Med. 2006; 12:841–845. [PubMed: 16767097]

Shao W, Espenshade PJ. Expanding roles for SREBP in metabolism. Cell Metab. 2012; 16:414–419. [PubMed: 23000402]

Uno K, Katagiri H, Yamada T, Ishigaki Y, Ogihara T, Imai J, Hasegawa Y, Gao J, Kaneko K, Iwasaki H, et al. Neuronal pathway from the liver modulates energy expenditure and systemic insulin sensitivity. Science. 2006; 312:1656–1659. [PubMed: 16778057]

Verberne AJ, Sabetghadam A, Korim WS. Neural pathways that control the glucose counterregulatory response. Front Neurosci. 2014; 8:38. [PubMed: 24616659]

Yi CX, la Fleur SE, Fliers E, Kalsbeek A. The role of the autonomic nervous liver innervation in the control of energy metabolism. Biochim Biophys Acta. 2010; 1802:416–431. [PubMed: 20060897]

Europe PMC Funders Author Manuscripts

Europe PMC Funders Author Manuscripts

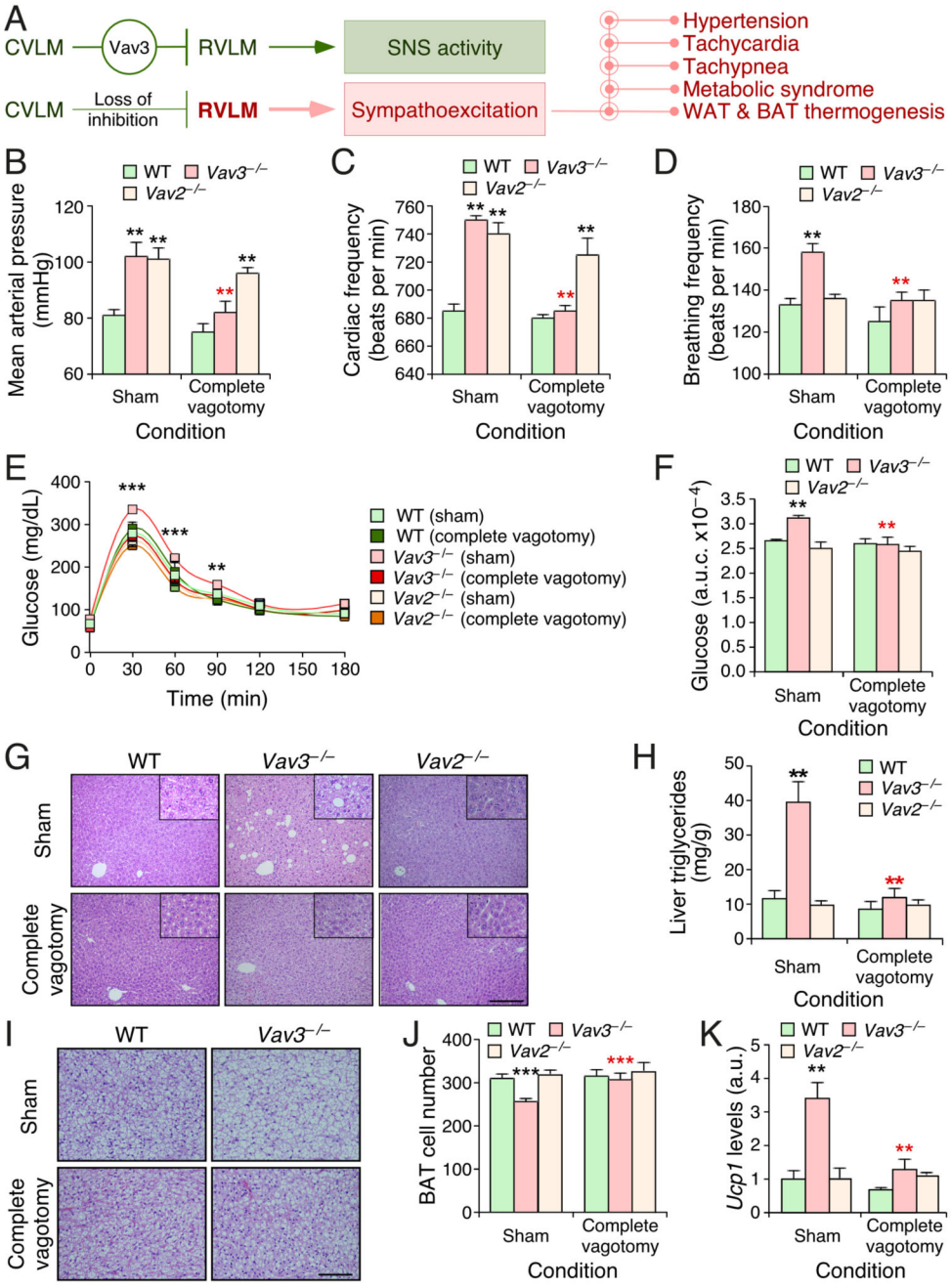

Figure 1. Complete subdiaphragmatic vagotomy blocks chronic sympathoexcitation–driven dysfunctions in mice

(A) Scheme of the regulatory status of the RVLM and downstream pathways in WT (green, top) and *Vav3*$^{-/-}$ (red, bottom) mice.

(B–D) Mean arterial pressure (B), heart frequency (C), and breathing ratio (D) of mice of indicated genotypes (inset) and experimental conditions (bottom).

(E) Glucose tolerance test in mice of indicated genotypes and experimental conditions.

(F) Area under the curve (a.u.c.) of the glucose tolerance tests performed in (E).

(G) Representative images of histological sections obtained from livers of mice of the indicated genotypes and experimental groups. Scale bar, 200 μm.
(H) Triglyceride content of livers from mice of the indicated genotypes and experimental groups.
(I) Representative histological images of interscapular BAT sections from mice of the indicated genotypes and experimental groups. Scale bar, 100 μm.
(J) Quantification of the number of brown adipocytes per field in interscapular BAT from mice of the indicated genotypes and experimental groups.
(K) Levels of indicated transcripts in the WAT from mice of indicated genotypes and experimental groups. Values are shown relative to the abundance of each transcript in the sham operated WT control (which was given an arbitrary value of 1). a.u., arbitrary number. Data shown in panels B–F, H, and J–K represent mean ± SEM. *, $P \leq 0.05$; **, $P \leq 0.01$; ***, $P \leq 0.001$ relative to either sham operated WT (black asterisks) or the sham operated animals of the same genotype group (red asterisks). Student's *t* and Mann–Whitney U tests were used for data obtained in panels (B–F,J) and (H,K), respectively. $n = 13$ (sham operated WT), 12 (sham operated *Vav3*$^{-/-}$ mice), 5 (sham operated *Vav2*$^{-/-}$ mice), 14 (vagotomized WT), 17 (vagotomized *Vav3*$^{-/-}$ mice), and 5 (vagotomized *Vav2*$^{-/-}$ mice).

Europe PMC Funders Author Manuscripts

Europe PMC Funders Author Manuscripts

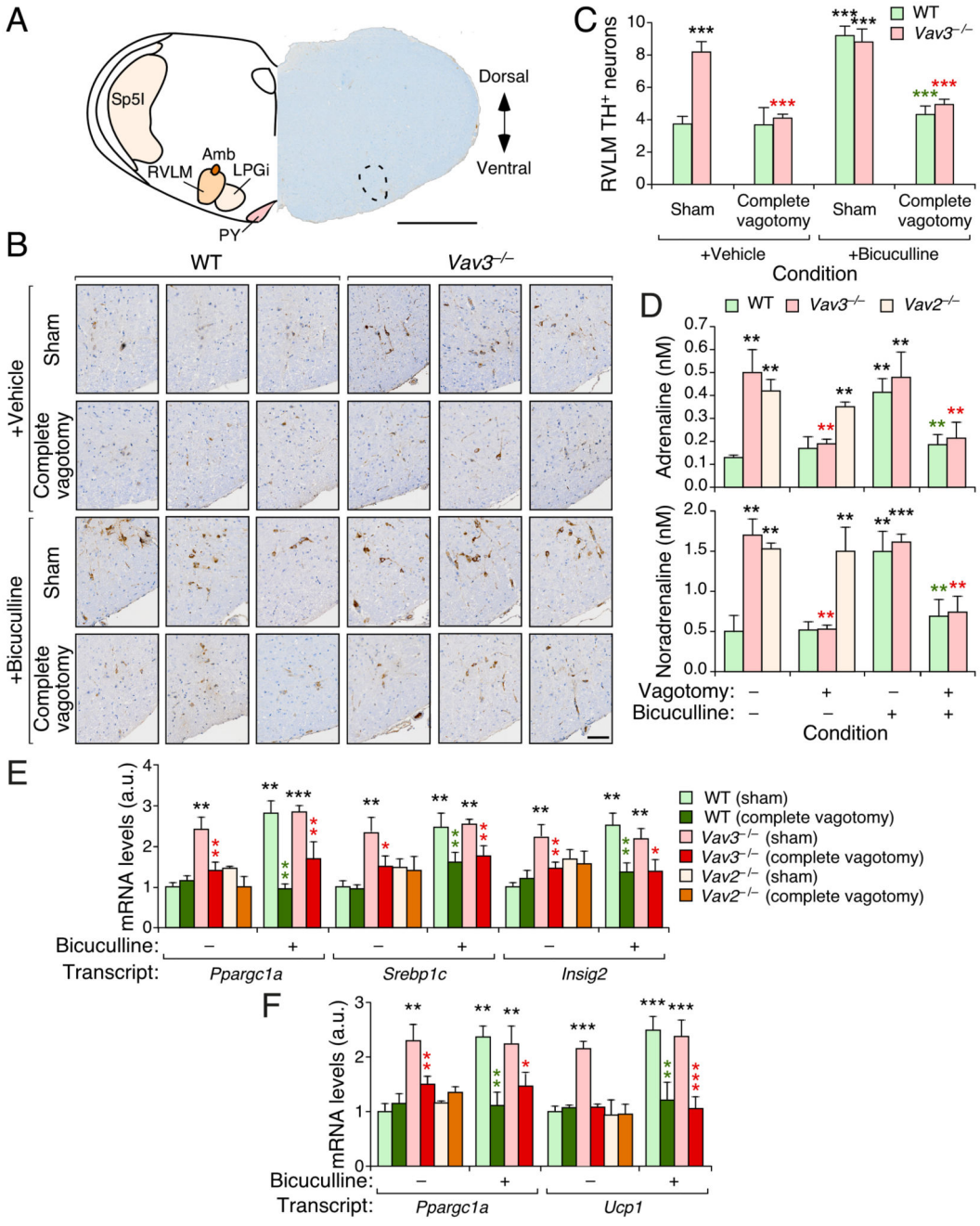

Figure 2. Vav3 deficiency–triggered RVLM hyperactivation requires vagal function

(A) Scheme (left) and representative (right) coronal brainstem section showing functional areas (left) and the specificity of TH staining within the RVLM (right, encircled area). Amb, nucleus ambiguus; LPGi, lateral paragigantocellular nucleus; PY, pyramidal tract; Sp5I, spinal trigeminal nucleus interpolar. D, dorsal; V, ventral. Scale bar, 1 mm.

(B) Representative immunohistochemical images showing TH^+ cells within the RVLM of mice of indicated genotypes and experimental groups. Scale bar, 100 μm.

(C) Quantification of the RVLM TH^+ cells from experiments shown in (B).

(D) Plasma catecholamine levels in mice of the indicated genotype, group and treatment.
(E,F) Abundance of the indicated transcripts in liver (E) and BAT (F) extracts from mice of indicated genotypes and experimental groups.
Data shown in panels C–F represent mean ± SEM. *, $P \leq 0.05$; **, $P \leq 0.01$; ***, $P \leq 0.001$ relative to either sham operated WT (black asterisks) or the sham operated animals of the same genotype group (red and green asterisks). ANOVA and Kruskal–Wallis tests were used for data obtained in panels (C,E,F) and (D), respectively. $n = 6$ (sham operated WT mice), 7 (sham operated WT + bicuculline), 6 (sham operated *Vav3*$^{-/-}$ mice with and without bicuculine), 7 (vagotomized WT with and without bicuculline), 8 (vagotomized *Vav3*$^{-/-}$ mice), 9 (vagotomized *Vav3*$^{-/-}$ mice + bicuculline), and 5 (sham operated and vagotomized *Vav2*$^{-/-}$ mice).

Europe PMC Funders Author Manuscripts

Europe PMC Funders Author Manuscripts

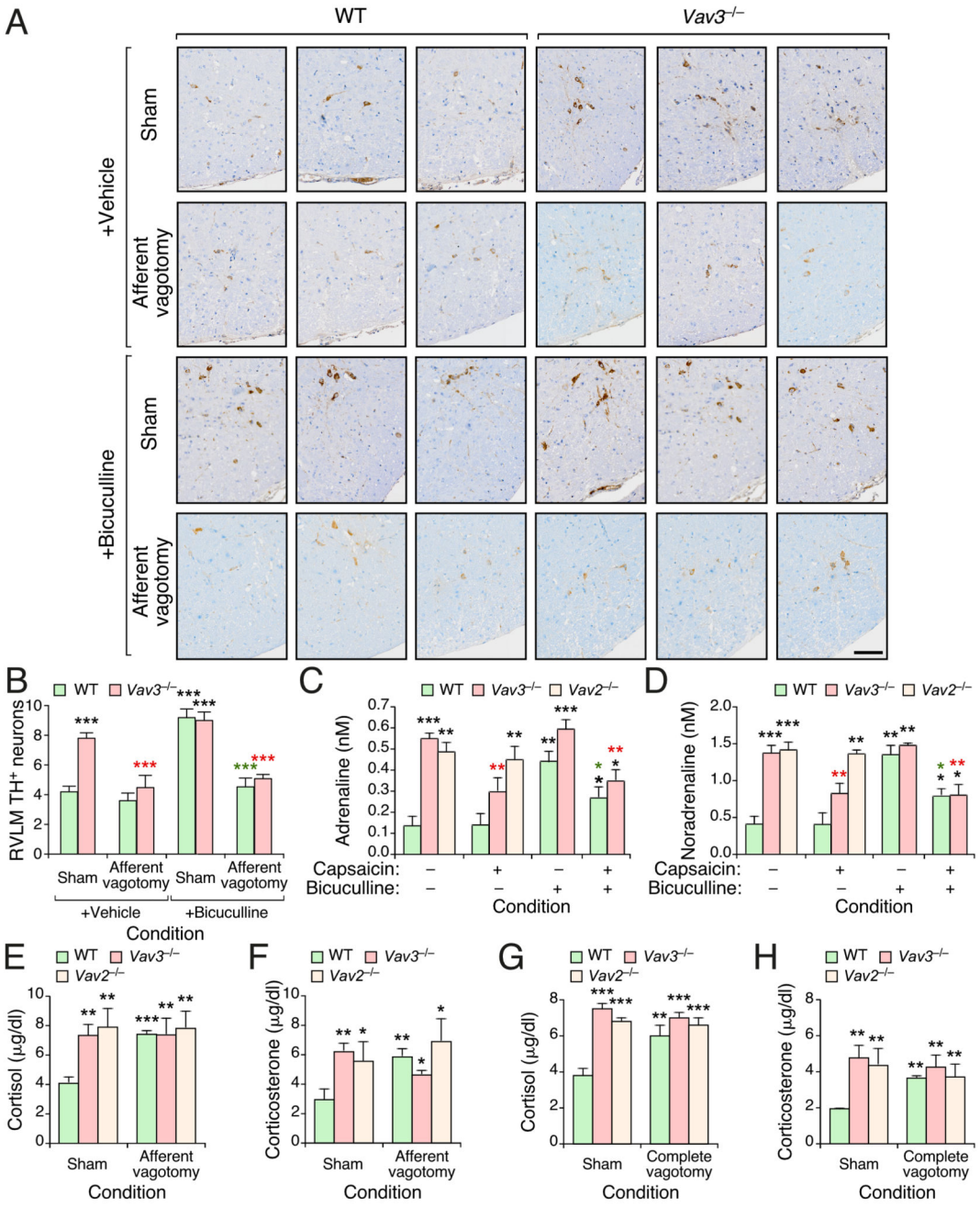

Figure 3. Vagal afferent fibers maintain RVLM–driven sympathoexcitation in *Vav3*$^{-/-}$ mice

(A) Representative immunohistochemical images showing TH^{+} cells within the RVLM of mice of indicated genotypes and experimental groups. Scale bar, 100 μm.

(B) Quantification of the RVLM TH^{+} cells from experiments shown in (A).

(C,D) Plasma adrenaline (C) and noradrenaline (D) levels in mice of indicated genotypes and experimental groups.

(E–H) Quantification of plasma cortisol (E,G) and corticosterone (F,H) levels in mice of indicated genotypes and experimental groups.

Data shown in panels B–H represent mean ± SEM. *, $P \leq 0.05$; **, $P \leq 0.01$; ***, $P \leq 0.001$ relative to either sham operated WT (black asterisks) or the sham operated animals of the same genotype group (red and green asterisks) ANOVA, Kruskal–Wallis, and Mann–Whitney U tests were used for data obtained in panels (B), (C,D), and (E–H), respectively. n = 5 (sham operated WT mice), 6 (sham operated WT mice + bicuculline), 5 (sham operated *Vav3*$^{-/-}$ mice), 6 (sham operated *Vav3*$^{-/-}$ mice + bicuculline, vagotomized WT with and without bicuculline), 7 (vagotomized *Vav3*$^{-/-}$ mice), 8 (vagotomized *Vav3*$^{-/-}$ mice + bicuculline), 5 (sham operated *Vav2*$^{-/-}$ mice), and 6 (vagotomized *Vav2*$^{-/-}$ mice) (panels B–F). n = 13 (sham operated WT mice), 12 (sham operated *Vav3*$^{-/-}$ mice), 5 (sham operated *Vav2*$^{-/-}$ mice), 14 (vagotomized WT mice), 17 (vagotomized *Vav3*$^{-/-}$ mice), and 5 (vagotomized *Vav2*$^{-/-}$ mice) (panels G–H).

Europe PMC Funders Author Manuscripts

Europe PMC Funders Author Manuscripts

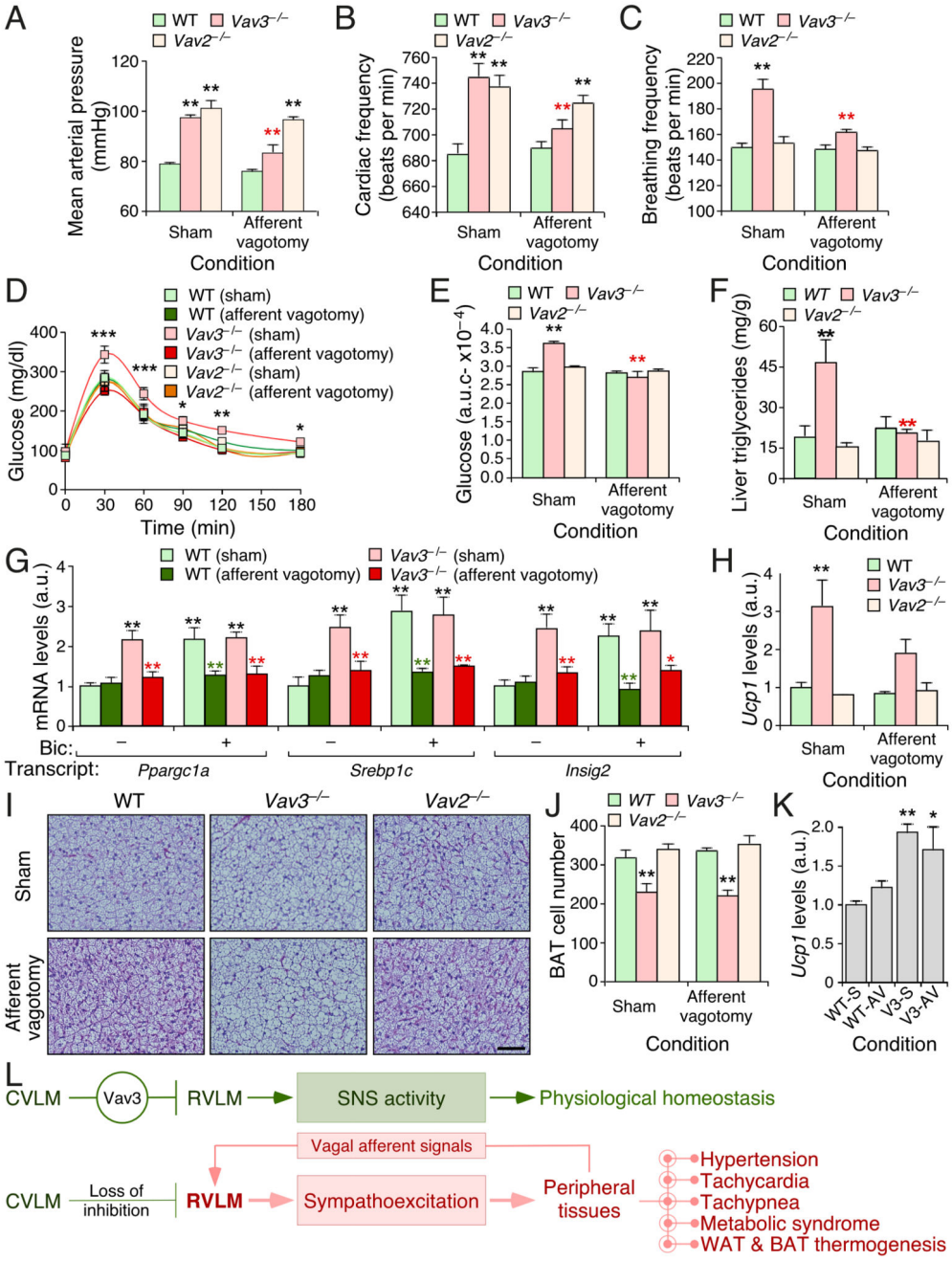

Figure 4. Afferent vagal fibers contribute to SNS–driven dysfunctions in *Vav3*$^{-/-}$ mice

(A–C) Mean arterial pressure (A), heart frequency (B), and breathing ratio (C) of mice of the indicated genotypes (inset) and experimental conditions (bottom).

(D) Glucose tolerance test of the animals of the indicated genotypes and experimental groups.

(E) Area under the curve values for the experiments shown in (D).

(F) Quantification of triglycerides in liver extracts from mice of the indicated genotypes and experimental groups.

(G,H) Abundance of the indicated transcripts in liver (G) and WAT (H) extracts from mice of the indicated genotypes and experimental groups. Bic, bicuculline.

(I) Representative histological images of interscapular BAT sections from mice of indicated genotypes and experimental groups. Scale bar = 100 μm.

(J) Quantification of the number of brown adipocytes per field in interscapular BAT from experiments shown in (I).

(K) Abundance of the indicated transcripts in BAT extracts from mice of the indicated genotypes and experimental groups. WT–S, sham operated WT mice; WT–AV, WT mice with afferent vagotomy; V3–S, sham operated *Vav3*$^{-/-}$ mice; Vav3–AV, *Vav3*$^{-/-}$ mice with afferent vagotomy.

(L) Summary of the results obtained in this work. Stimulatory and inhibitory connections are depicted as arrows and blunted lines, respectively.

Data shown in panels A–H, J and K represent mean ± SEM. *, $P \leq 0.05$; **, $P \leq 0.01$; ***, $P \leq 0.001$ relative to either sham operated WT (black asterisks) or the sham operated animals of the same genotype group (red and green asterisks). Student's *t*, ANOVA, and Mann–Whitney U tests were used for data obtained in panels (A–E,J), (G), and (F,H,K), respectively. $n = 11$ (sham operated WT mice), 11 (sham operated *Vav3*$^{-/-}$ mice), 5 (sham operated *Vav2*$^{-/-}$ mice), 12 (vagotomized WT mice), 15 (vagotomized *Vav3*$^{-/-}$ mice), 6 (vagotomized *Vav2*$^{-/-}$ mice).